Effects of Ingested Atmospheric Turbulence on Measured Tail Rotor Acoustics

David B. Signor

Gloria K. Yamauchi

Marianne Mosher

NASA Ames Research Center
Moffett Field, CA

Martin J. Hagen
Kenetech Windpower
Livermore, CA

Albert R. George
Cornell University
Ithaca, NY

Results from an outdoor hover test of a full-scale Lynx tail rotor are presented. The investigation was designed to further the understanding of the acoustics of an isolated tail rotor hovering out-of-ground effect in atmospheric turbulence, without the effects of the main rotor wake or other helicopter components. Measurements include simultaneous rotor performance, noise, inflow, and far-field atmospheric turbulence. Results with grid-generated inflow turbulence are also presented. The effects of atmospheric turbulence ingestion on rotor noise are quantified. In contradiction to current linear theories, increasing rotor inflow and rotor thrust were found to increase turbulence ingestion noise.

Notation

a	speed of sound, m/s
A	autocorrelation coefficient
b	number of blades (4)
c	blade chord (0.18 m)
C_T/σ	rotor thrust coefficient divided by rotor solidity, rotor thrust/$R\rho(\Omega R)^2bc$
dBA	A-weighted Sound Pressure Level (referenced to 20 μPa)
d	separation distance between rods in the turbulence-generating grid (7.6 cm)
g	distance downstream from grid, cm
g_0	position of maximum grid-generated turbulence ($5 \le \frac{g_0}{d} \le 15$), cm
M_{tip}	rotor tip Mach number, $\Omega R/a$
N	number of data samples per hot-film time record (2048)
OASPL	Over All Sound Pressure Level, dB (referenced to 20 μPa)
O_r	observer radial distance normalized by R
R	rotor radius (1.105 m)
u'	rms turbulence velocity, , m/s
$\bar{u}$	average velocity, , m/s
U	velocity measured by hot-film probe, m/s
U_∞	atmospheric wind speed measured by cup anemometer, m/s
V_{rot}	inflow velocity measured by pitot probe, m/s
x	x-direction, +x is in the direction of the rotor wake, right-hand coordinate system (x=0 is at the rotor plane)
y	y-direction (y=0 is at the rotor axis)
z	z-direction, +z is upwards from the ground (z=0 is at the ground)
z_{hub}	height of rotor hub above ground, (6.1 m)
Δt	hot-film signal sample spacing (0.0125 s)
γ	atmospheric wind direction measured from rotor axis (positive, clockwise looking down), deg
Λ	eddy length, m
Ω	rotor rotational speed, rad/s
ρ	air density, kg/m^3
τ	autocorrelation delay, $\tau = j\Delta t$, s

Subscripts;

f	denotes far-field hot-film parameter
n	denotes near-field hot-film parameter
i	the ith sample in the calculation of eddy length, $0 \le i < N-1$
j	the jth sample in the calculation of eddy length, $0 \le j < N$

This paper is a modified version of the paper presented at the American Helicopter Society Forum, Washington, D.C., June 3-5, 1992.

Received Oct. 1994; accepted Oct. 1995.

Introduction

Turbulence ingestion noise is an important source of helicopter noise, particularly in the absence of impulsive noise sources (Ref. 1), and can be a significant source of broadband noise when a helicopter is in hover or vertical ascent (Ref. 2). Turbulence ingestion noise is generated when a rotor blade interacts with atmospheric turbulence or the turbulent wakes of preceding blades (Ref. 2). For a lifting, hovering rotor, however, the wake of the preceding blade will convect out of the path of the following blades, leaving the atmospheric turbulence as a major contributor to the sound radiated by a hovering rotor. The manner in which ingested atmospheric turbulence is manifested as rotor noise is explained as follows. A lifting rotor accelerates the air and stretches atmospheric eddies passing through the rotor. The velocity fluctuations in the eddies cause fluctuations of the local pressure, lift, and drag of the rotor blades. These unsteady forces are the acoustic source of atmospheric turbulence ingestion noise. A blade-eddy interaction produces broadband noise. Multiple interactions with a single eddy produce correlated disturbances. The blades of a hovering tail rotor can chop an atmospheric eddy over 500 times. The exact number of chops depends on the number of blades, rotor rpm, eddy size, and rotor inflow velocity. For a hovering main rotor, the blades chop a single atmospheric eddy 10 to 200 times. Acoustic spectra from a tail rotor chopping atmospheric turbulence will be narrow band. Acoustic spectra from a main rotor chopping atmospheric turbulence will contain both narrow band and broadband components.

In order to determine the effects of atmospheric turbulence ingestion on rotor acoustics, numerous characteristics of the atmosphere must be measured simultaneously, in addition to the rotor-radiated noise. To date, no single experiment has included acquisition of all the necessary but difficult measurements. Unlike the controlled environment in a wind tunnel, the atmosphere is inherently unsteady and at times unstable. A large number of assorted sensors located at various altitudes would be required to thoroughly document the changing atmospheric conditions.

Complete characterization of the atmospheric turbulence was beyond the scope of this experiment. The objective of this experimental investigation was to correlate a few basic features of atmospheric turbulence with the sound radiated by a full-scale Lynx tail rotor in hover. Additional data from the experiment are presented in Ref. 3. This paper presents selected measurements of simultaneous rotor performance, noise, inflow, and far-field atmospheric turbulence. Results with grid-generated turbulence are also presented.

Description of Experiment

Model

A full-scale Lynx tail rotor was used for this investigation. This rotor consists of four constant-chord, untwisted blades (Ref. 3). Nominal rotor speed was 1850 rpm, 214 m/s tip speed. The rotor hub has conventional flapping and feathering hinges and was installed 6.1 m above the ground. The tail rotor was mounted on the NASA Ames Tail Rotor Test Rig (TRTR), shown in Fig. 1, at the Outdoor Aerodynamic Research Facility. The rotor drive motor, drive shaft, and right-angle gearbox are mounted inside the horizontal boom, which is mounted on the main vertical support. The turbulence generating grid is shown in Fig. 1. During the testing, the rotor was typically operated such that the inflow was drawn through the grid, (and the wake would be flowing out-of-the-page as viewed in Fig. 1). Additional information about the TRTR, Lynx tail rotor, and previous test results are found in References 3 - 7.

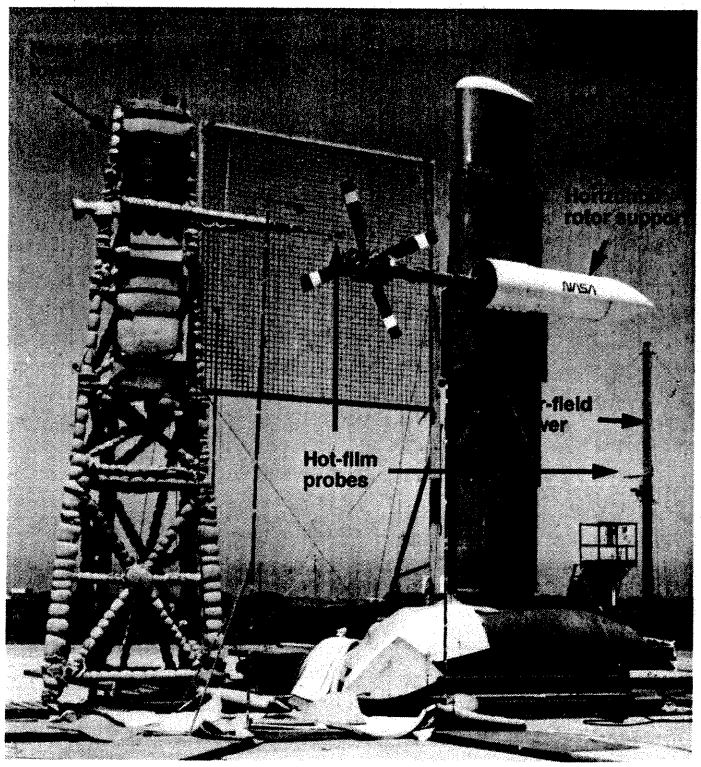

Rotor Measurements

A strain-gauge balance was used to measure the mean rotor thrust, torque, and vertical force. The balance was mounted between the horizontal support tube and the gearbox mounting bracket. Rotor balance data were acquired using a low-pass filter set at 10 Hz. Mean blade flapwise bending moments were measured at 30%, 40% and 70% radial positions. Bending moment data were acquired using a low-pass filter set at 100 Hz. Mean balance and blade bending moment data were computed from 15 s of data.

Flow Measurements

The rotor inflow was measured with a single-element hot-film anemometer and a pitot-static probe. Both these probes were located immediately upstream of the rotor. Data from the pitot-static probe were low-pass filtered with the filter set at 10 Hz; averaged values were computed from 15 s of data. The hot-film and pitot-static probes were mounted on a tower and remained fixed relative to the rotor. The hot-film was horizontal and parallel to the rotor plane.

A 3.6- by 3.6- m turbulence-generating grid was installed upstream of the rotor for several runs. The grid consisted of 1.3 cm diameter rods arranged in 7.6 cm square cells. The grid changed the character of the ingested turbulence by introducing small-scale turbulence. Fig. 2 shows the locations of the hot-film probe and grid with respect to the rotor (a right-hand coordinate system is used as shown in Figs. 2 and 3). According to Hinze (Ref. 8) and Batchelor (Ref. 9), grid-generated turbulence becomes homogeneous in a uniform freestream for $g/d \geq 10$, where g is the distance downstream from the grid and d is the cell width. At $g/d=10$, maximum turbulence velocity is expected. The hot-film and rotor plane were positioned at $g/d=9.5$ and $g/d=16.7$, respectively. The flow into the grid is recognized as non-uniform since the rotor inflow has spanwise variations in axial velocity. However, the methods of Batchelor (Ref. 9) were used to position the grid upstream of the rotor; therefore, the turbulence at the rotor plane is assumed to be homogeneous.

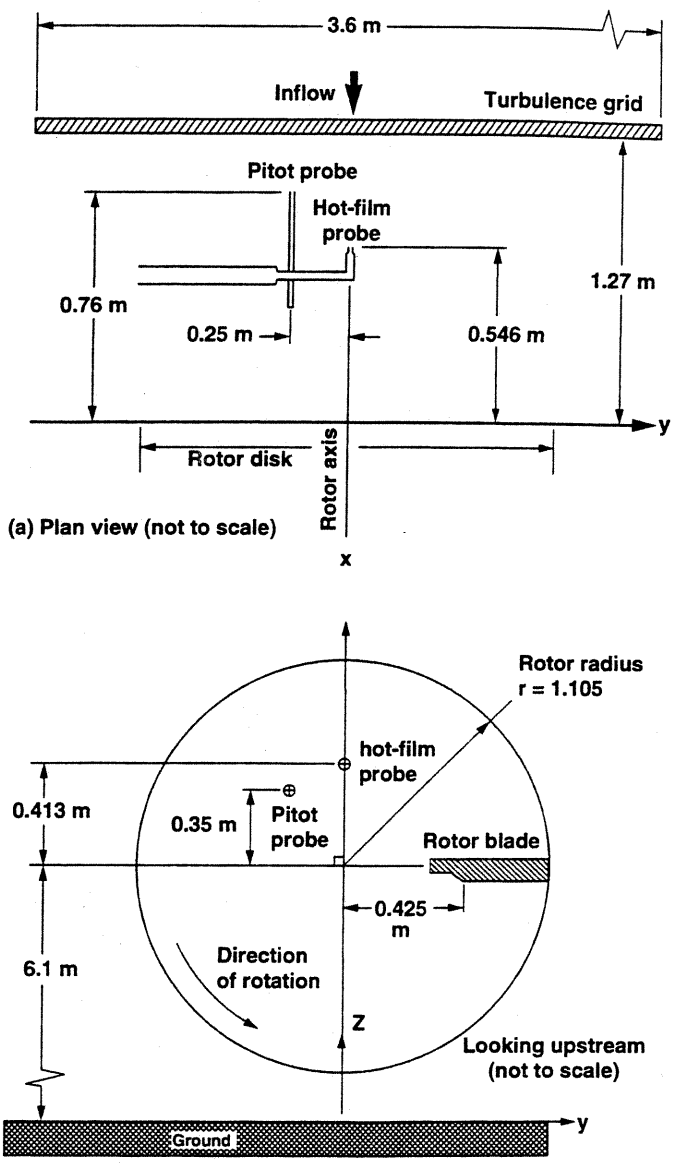

Fig. 2. Near-field hot-film probe and grid location.

A second single-element hot-film was mounted on a tower located upstream and to the side of the tail rotor. The hot-film was horizontal and parallel to the rotor plane. The probe was located at z=4.7 m and remained fixed. This probe was used to measure the atmospheric turbulence in the far-field. Fig. 3 shows the location of the far-field tower with respect to the rotor. The near-field pitot-static and hot-film probes are too small to be shown clearly in Fig. 3, but they are mounted on the support arm of the near-field tower immediately upstream of the rotor (also shown in Fig. 1).

Constant temperature anemometer bridges powered the hot-film probes. The anemometer signals were linearized. The near-field probe signal was low-pass filtered (filter set at 40 Hz) to remove the blade passage frequency before being digitized. A dynamic signal analyzer with an anti-aliasing filter was used to digitize the data from both probes. No averaging or windowing was used. The data were recorded for 25.6 s at 80 samples/s. The probes were calibrated before the experiment, but not before every run. A second calibration performed after the

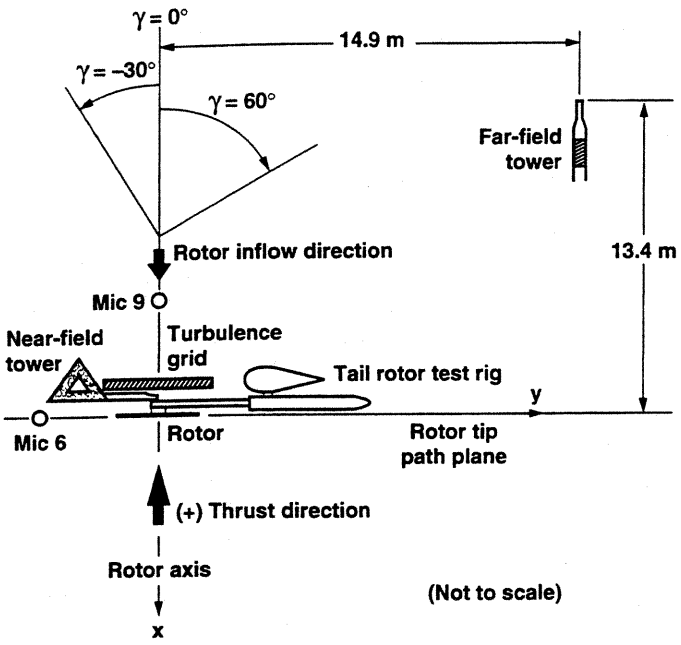

Fig. 3. Plan view of experimental set-up.

completion of the experiment revealed very little change in the probes' conversion constants and offsets. The data were reduced using the average of the results from the two calibrations.

Atmospheric wind speed and direction were measured using a cup anemometer and a weather vane located on a third tower roughly 46 m upstream of the rotor, 55 m from the rotor axis, and 10 m above the ground (x=-46m, y=55m, z=10m). Additionally, the weather station at Naval Air Station Moffett Field recorded several atmospheric parameters hourly. Measurements included air temperature, wind speed, wind direction, barometric pressure, humidity, and cloud conditions. These measurements were recorded 12.8 m above sea level, at a location approximately 1500 m south-east (approximately on the x = y vector) of the Outdoor Aerodynamic Research Facility.

Acoustic Measurements

Five microphones were typically used to acquire acoustic data. The microphones were placed in an array about the rotor at distances of 2.5, 4.5, and 10 rotor radii away from the hub. Data from two microphones (mic 6 and mic 9) are presented in this paper. The location of mic 6 and mic 9 are described in Table 1 and Fig. 3. Data from the other microphones are presented in Ref. 3. Acoustic foam was used to substantially reduce reflected rotor noise off the ground, near-field tower, and TRTR (Fig. 1). Wind screens were placed over each microphone to reduce wind-generated noise.

The microphones were calibrated daily using a pistonphone. Two microphone calibrations were recorded each day. The conversion con-

Table 1. Microphone Locations

Microphone	O_T	γ (deg)	$(z-z_{hub})/R$
No. 6	4.5	270	0.0
No. 9	4.5	0	0.0

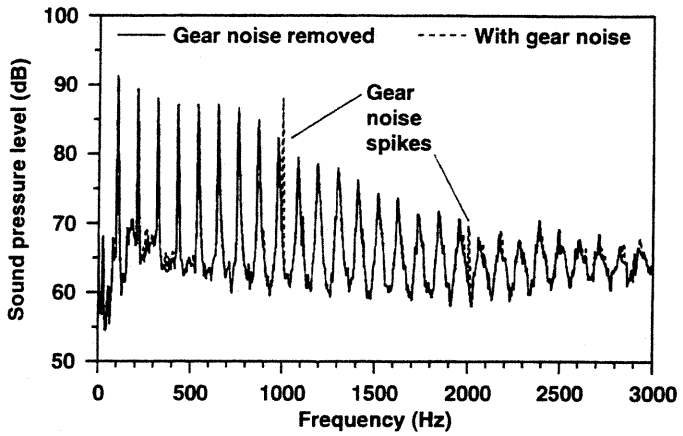

Fig. 4. Power spectrum showing effect of gear noise removal at microphone 9, O_r = 4.5, Run 44 Point 5, M_{tip} = 0.56, θ = 11°, U_∞ = 0.00 m/s, near field-tower not installed, grid not installed.

stants from the two recorded calibrations were then averaged; this averaged value served as the conversion constant for each microphone for that particular day. The error associated with this method is on the order of +_1 dB. The data were recorded for 30 s using a 14-track FM tape recorder with a tape speed of 30 ips, giving a frequency range of 20 kHz. Spectra from the acoustic time histories were generated by a dynamic signal analyzer using the rotor 1/rev as an external trigger. The fluctuation in rotor speed was less than 0.2 percent of full-scale, that is, no more than 2 to 4 rpm. All acoustic data were reduced using a time record of 0.256 s per average (approximately 8 revolutions per average based on a nominal rpm of 1850), a span of 3.125 kHz, and a bandwidth of 5.86 Hz. Each spectrum represents 25 averages (no overlap) of power spectra made with a Hanning window.

The measurements of rotor noise include gear noise from the right-angle gearbox located immediately upstream of the rotor hub. Gear noise, as described by Dale (Ref. 10), appears in the spectra as discrete frequency spikes at some sidebands of the integer harmonics of the gear mesh frequency (37/rev) modulated by the rotor blade passage frequency (k*37 ± n*4 per rev, k and n are integers). The probable cause is modulation of the gear mesh frequency by quasi-periodic disturbances on the rotor blades. Noise was not produced at all sidebands. Gear noise was removed from the spectra for sidebands of the first three harmonics of the gear mesh frequency. The following procedure was used to remove the gear noise. A low-order polynomial curve was fit through the 80% dB levels of a noise spectrum. Next, frequencies (k*37 ± n*4 per rev) contaminated with gear noise were identified. Amplitudes at these contaminated frequencies were removed if the amplitude exceeded the polynomial curve fit value. The amplitude was then replaced with an interpolated value using frequencies (with amplitudes less than the curve fit value) adjacent to the contaminated frequency. This procedure generally reduced amplitudes at three or four spectral lines centered at the contaminated frequency. A typical correction to an acoustic spectrum is shown in Fig. 4. Note that the gear noise spikes at 1000 Hz and 2000 Hz have been removed, while the remainder of the spectrum has not been altered.

Configuration and Test Envelope

Data acquisition times were planned for morning hours when the wind speed at the site was low, generally below 2 m/s (with some data acquired between 2 and 6 m/s), in order to simulate hover and obtain high quality acoustic data. The low winds led to generally low turbulence intensities.

The test configuration consisted of the TRTR with the microphone array and the near-field and far-field towers. Data were also acquired prior to the installation of the towers. In addition, the turbulence grid was installed for some of the data acquisition runs. The ranges of test parameters are shown in Table 2.

Data Quality

In analyzing the large amount of acoustic and turbulence data, every effort was made to exclude questionable data. Criteria for excluding data and quality of the data are discussed below.

Table 2. Ranges of Test Parameters.

Configuration:	No Tower; No Grid	Tower; No Grid	Tower; Grid
Rotor collective pitch	-9° to 15°	3° to 15°	3° to 15°
C_T/σ	-0.0296 to 0.0789	0.0038 to 0.0758	0.0041 to 0.0760
Rotor tip Mach number, M_{tip}	0.52 to 0.63	0.52 to 0.62	0.62
Atmospheric wind direction, γ	*	-28° to 59°	-17° to 59°
Atmospheric wind speed, U_∞ (m/s)	0.0 to 2.67	0.38 to 5.74	1.27 to 3.57
Far-field eddy length, Λ_f (m)	-	0.8 to 12.8	1.0 to 14.1
Average inflow velocity, $\bar{u}_n$ (m/s)	-	2.24 to 8.71	2.84 to 11.40

* Includes conditions for which $U_\infty \leq 1.0$ m/s regardless of atmospheric wind direction and conditions for which $-30° \leq \gamma \leq 60°$ regardless of atmospheric wind speed.

Atmospheric Measurements

The data were limited to those conditions acquired with wind directions of $-30° \le \gamma \le 60°$ (Fig. 3) for the runs in which the near-field tower was present. This avoided blockage effects from the near-field tower and the TRTR on the rotor and hot-film measurements. For those runs conducted prior to the near-field tower installation, the data were limited to the same wind direction envelope or those conditions in which the ambient wind speed was less than 1.0 m/s, regardless of wind direction.

The longitudinal eddy lengths at the near-field and far-field locations were obtained from respective fixed hot-film probe autocorrelations. The autocorrelation is defined as

$$A_j = \frac{1}{N-j} \sum_{i=1}^{N-j} (U_i - \bar{u})(U_{i+j} - \bar{u})$$

The eddy lengths are defined by

$$\Lambda_n = \bar{u}_n \, \Delta t \sum_{j=0}^{q-1} \frac{A_{nj}}{A_{n0}}$$

$$\Lambda_f = \frac{\bar{u}_f}{\cos\gamma} \, \Delta t \sum_{j=0}^{q-1} \frac{A_{fj}}{A_{f0}}$$

where q is the integer for which Aj first becomes negative for a given time history. Although Aj is defined for $\phi \le j < N$, only the information in the range $\phi \le j < q$ is actually used. Time histories whose autocorrelations did not change sign were considered non-stochastic, and thus were not included. The far-field eddy lengths were computed using the $(\cos\gamma)$ factor to account for wind direction.

As stated earlier, the probe signals were recorded for 25.6 s. A time record of perhaps thirty minutes for the far-field probes would have been better for determining if the flow was stationary, since the far-field contains turbulent eddies which are complex, large-scale structures. Because the time record lengths were insufficient to obtain statistically accurate autocorrelations and integral times, the integral scales presented should be considered only as rather coarse estimates.

In addition, a higher sampling rate for the hot-film probes would have been preferable, especially for the near-tower probe. Since the probe signals were sampled at 80 samples/s and the near-tower signal was low-pass filtered at 40 Hz before being recorded, the frequency content beyond 40 Hz is not available. This prevents a determination of the turbulence spectrum above 40 Hz and precludes a determination of the filter effect on the turbulence level or length scale. In a similar experiment, however, Paterson and Amiet (Ref. 11) found the error in overall rms turbulence level due to low-pass filtering to be less than 10%. Instrumentation limitations dictated that only a fixed number of samples (2048 samples) could be acquired per channel per data point, leading to the chosen compromise between record length and sample rate (2048 samples / 80 samples/sec = 25.6 seconds).

As a means of verifying the rotor inflow velocity measured by the hot-film, a pitot-static probe was placed in the rotor inflow. The pitot-static probe was slightly (4%) closer to the blade tip than the hot-film (Fig. 2). Rotor inflow surveys performed by Simonich, et al (Ref. 12) indicate that the magnitude of the inflow velocity increases with distance from the center of rotation to roughly 60% of the blade radius, so the pitot-static probe is expected to experience somewhat higher inflow velocities than the hot-film. The pitot-static probe velocity (V_{rot}) is shown plotted against the hot-film velocity ($\bar{u}_n$) for several rotor collective pitch settings in Fig. 5. The slope of the data in Fig. 5 is greater than unity, and therefore the inflow velocity measured by the hot-film probe is considered consistent with that measured by the pitot-static probe.

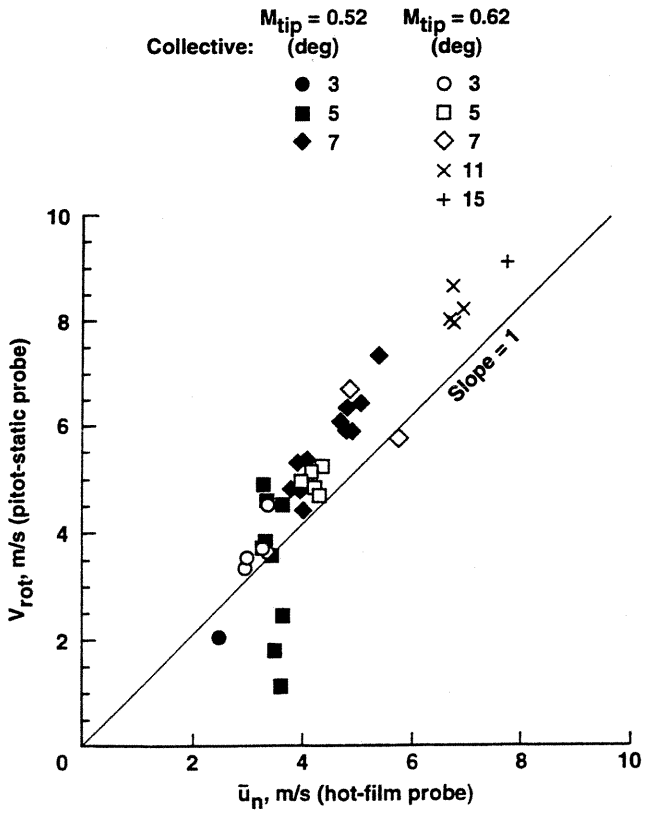

Fig. 5. Comparison of rotor inflow velocity, measured by the pilot-static probe and the hot-film probe.

Acoustic Measurements

As stated earlier, data are limited to a narrow range of wind directions for those runs in which the near-field tower was present to minimize the influence of the near-field tower on the rotor inflow. However, acoustic reflections from the tower were a concern since not all of the tower could be treated with foam and the foam does not completely eliminate reflections. Data were acquired early in the experimental program without the tower installed. These data are limited to the same wind direction envelope, or to those conditions in which the ambient wind speed was less than 1.0 m/s regardless of wind direction. Comparisons are made of acoustic spectra with and without the tower in Fig. 6. Rotor and atmospheric conditions are similar, but not exact. Note that the rotor rpm is 1.5% higher for the condition with the tower present. Both microphone spectra, especially the in-plane microphone spectrum (mic 6, Fig. 6(a)), exhibit slightly higher floors at the higher frequencies in addition to higher blade passage harmonic peaks with the tower present. Because of the inherent difficulty in obtaining closely matched atmospheric conditions with and without the tower present, only one comparison is possible among the data set to assess the influence of the tower. Fig. 6(b), shows that the presence of the tower does not dramatically change the character of the acoustic spectrum of the on-axis microphone, where turbulence ingestion noise is most dominant. We conclude, then, that the turbulence ingestion noise measured by the on-axis microphone is not significantly influenced by the presence of the tower.

Another structure which may have disrupted the inflow to the rotor is the horizontal rotor support structure. For positive thrust, the horizontal support is immediately upstream of the rotor. The support could

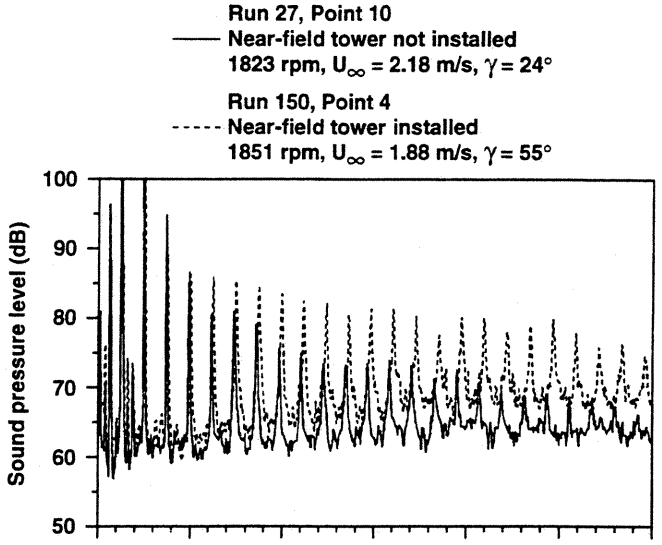

(a) Microphone 6

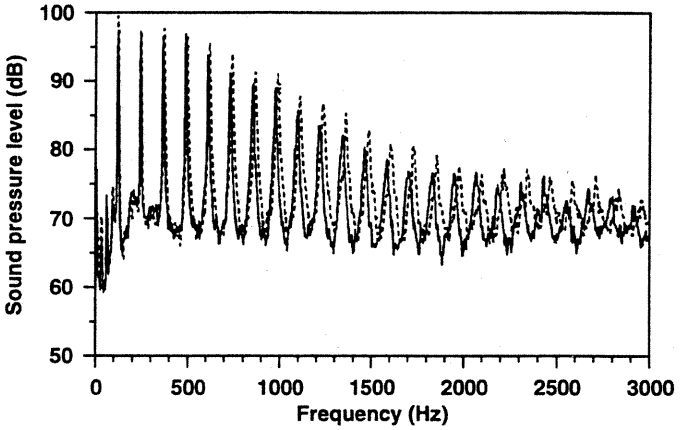

(b) Microphone 9

Fig. 6. Effect of near-field tower on acoustic power spectra for θ = 15°, grid not installed. (a) Microphone 6, (b) Microphone 9.

generate disturbances in the flow which produce noise similar to noise produced by ingested atmospheric turbulence. This possibility was investigated by looking at the acoustic spectra for a low wind, negative thrust condition, and a corresponding positive thrust condition. For a negative thrust condition, the horizontal support is in the wake of the rotor rather than in the inflow. The character of the spectra were found to be similar for the positive and negative thrust conditions. Thus even when the horizontal support is not in the rotor inflow, turbulence ingestion noise exists. Since there are no other structures which could disturb the inflow of the rotor for a negative thrust condition, the turbulence ingestion noise is attributed to atmospheric turbulence. Therefore, any turbulence ingestion noise caused by the horizontal support for positive thrust conditions is reasoned to be small compared to the atmospheric turbulence ingestion noise.

Data consistency and repeatability are important qualities of any experiment but can be difficult to achieve in an outdoor test. The atmospheric conditions usually remained fairly steady during a run, although the occurrence of a wind gust or changes in ambient noise levels during

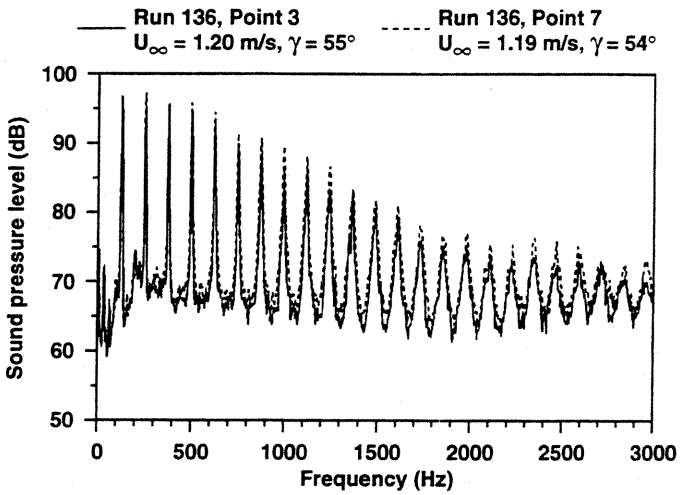

Fig. 7. Consistency of acoustic power spectra for θ = 11°, M_{tip} = 0.62, near-field tower installed, grid not installed, microphone 9.

data acquisition were possible. The degree of data repeatability is shown in Fig. 7 (mic 9). Runs for this experiment typically lasted 20 to 30 minutes. Rotor rotational velocity was adjusted between data point acquisitions as necessary to maintain a specified value of M_{tip}, and is the only rotor operating control which was varied in a given run. The atmospheric wind speed and direction change slightly within a run. The on-axis microphone result is very repeatable. Fig. 7 represents the amount of scatter to be expected in the on-axis microphone acoustic spectra.

Results and Discussion

Data characterizing the atmospheric turbulence are discussed first. The sensitivity of the acoustic measurements to basic characteristics of the atmospheric turbulence are then discussed.

Atmospheric Measurements

Quantifying the magnitude of turbulence ingestion noise for this test requires detailed knowledge of the atmospheric turbulence structure, which is very complicated. The structure depends upon the wind profile and upstream conditions, terrain roughness and shear, fluxes of moisture and thermal energy, cloud cover, and other factors. Depending on these factors the turbulence velocities can be moderately or severely anisotropic (especially in stable, stratified conditions). Additionally, non-homogeneous large eddy structures often include significant intermittency (Refs. 13 and 14), and the rotor distorts the environmental turbulence (Ref. 15). However, for the purpose of this paper, the atmosphere is assumed to be isotropic far from the rotor.

The upstream wind conditions at the Outdoor Aerodynamic Research Facility generally begin over San Francisco Bay. From the shoreline, the upstream wind flows over a kilometer of terrain consisting of long grass with some shrubs, isolated trees, and berms. Although the atmosphere appeared to be stably stratified at higher altitudes, the atmosphere at the rotor height was likely neutral or slightly unstable during the testing periods due to mechanical mixing from terrain roughness. The general character of the turbulence at any location in the atmospheric boundary layer is determined by the stability of the atmosphere relative to the turbulence generated by shear stress. If the atmosphere is neutral to slightly buoyant the turbulence will be similar to that in an aerodynamic boundary layer. Following Panofsky and Dutton (Ref. 16), the degree of atmospheric buoyancy was examined for the atmospheric

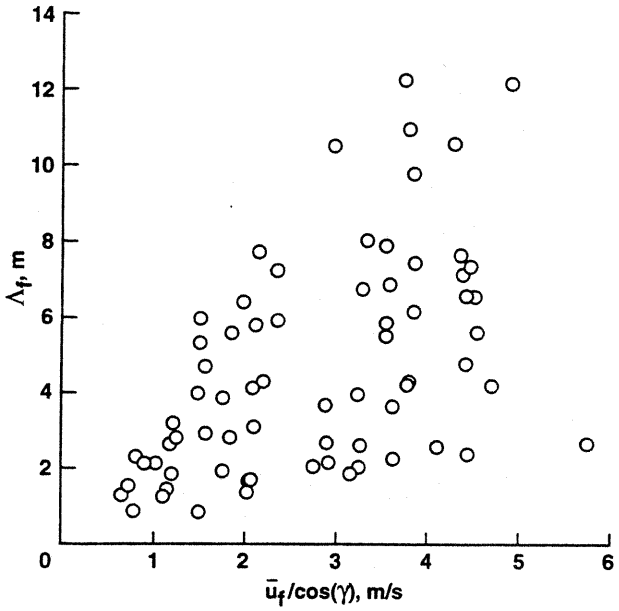

Fig. 8. Far-field eddy lengths.

conditions which occurred during this test by estimating the Turner classes of the flow from the Moffett Field weather and solar data to find the approximate Monin-Obukhov lengths and Richardson numbers. The range of estimated Monin-Obukhov lengths was approximately -10 to -25 m and the range of Richardson numbers was approximately -0.06 to -0.25, indicating near neutral to slightly unstable conditions. This was consistent with the hot-film measurements and indicates that the assumption of isotropic turbulence is a reasonable first approximation far from the rotor.

Far-Field. Far-field turbulence length scales of the largest eddies are shown in Fig. 8 to increase as a function of the atmospheric wind speed. The wind speed component measured by the far-field probe has been adjusted for wind direction in order to arrive at the total magnitude. The eddy lengths at the lowest wind speeds are small because there is little mechanical mixing of the atmospheric boundary layer. The eddy lengths initially increase with increasing wind speed, but become less dependent on wind speed at moderate wind speeds. At higher wind speeds, the largest length scales are of the order of the measurement height (z = 4.7 m), consistent with length scales that are expected for a neutral to slightly buoyant boundary layer. Length scales less than the largest length scale are observed at all wind speeds.

The normalized atmospheric rms turbulence velocities, u'_f/U_∞ shown in Fig. 9, are independent of atmospheric wind speed, as expected.

Near-Field. The ratio of near- to far-field longitudinal eddy lengths, shown in Fig. 10, is a measure of the stretching of the eddies as they are accelerated through the rotor. The grid was not installed for these conditions. The amount of eddy stretching, as the eddies are accelerated through the rotor, is one measure of how the rotor alters the surrounding atmospheric turbulence prior to ingesting the turbulence. The length and speed of the ingested eddies determines the number of times the eddy will be chopped by the rotor blades. The ratio of near- to far-field longitudinal eddy lengths is generally, but not always, greater than unity. This is because the measurements were made in an Eulerian sense, not Lagrangian; individual eddies were not tracked as they traveled from the far-field and became distorted by the rotor. Therefore, the eddies entering the rotor should in general be longer than the far-field eddies, but there can be exceptions. Length scales of the ingested eddies are shown in Fig. 11 as a function of the inflow velocity. The scatter in the data is large; no discernible effects of M_{tip} or rotor collective pitch on eddy length were observed.

Fig. 12 shows ingested rms turbulence velocity as a function of atmospheric wind speed. The normalized rms turbulence velocity is independent of atmospheric wind speed. Also, there is no discernible effect of rotor operating condition (M_{tip} or C_T) on rms turbulence velocity.

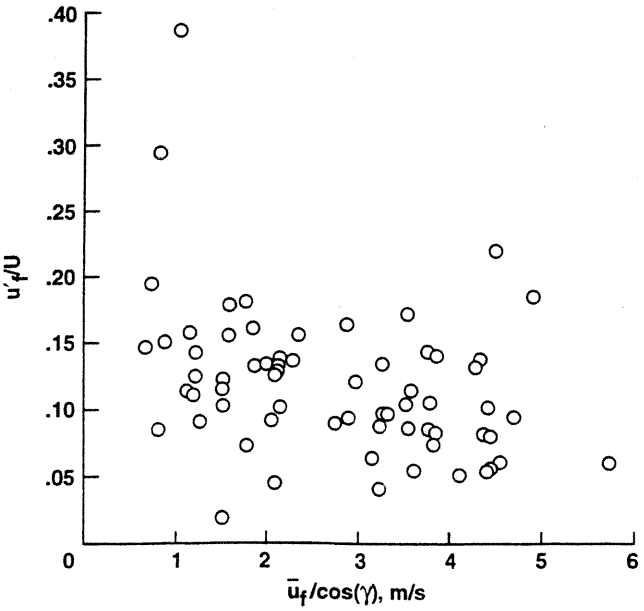

Fig. 9. Far-field rms turbulence velocity.

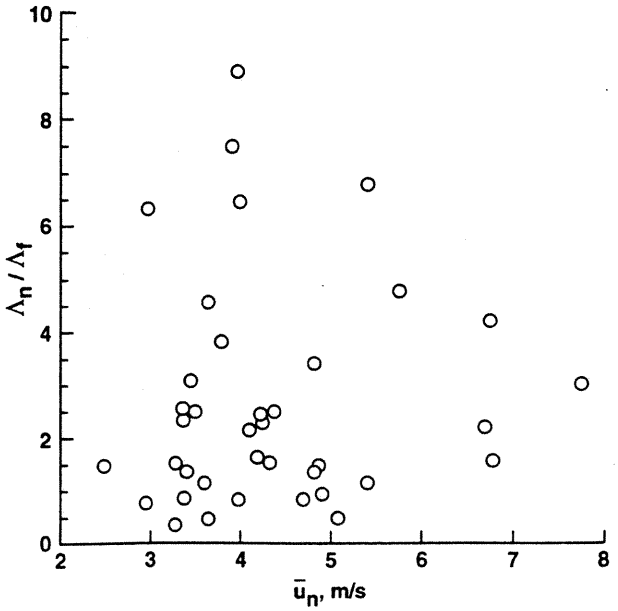

Fig. 10. Longitudinal eddy length stretching ratio.

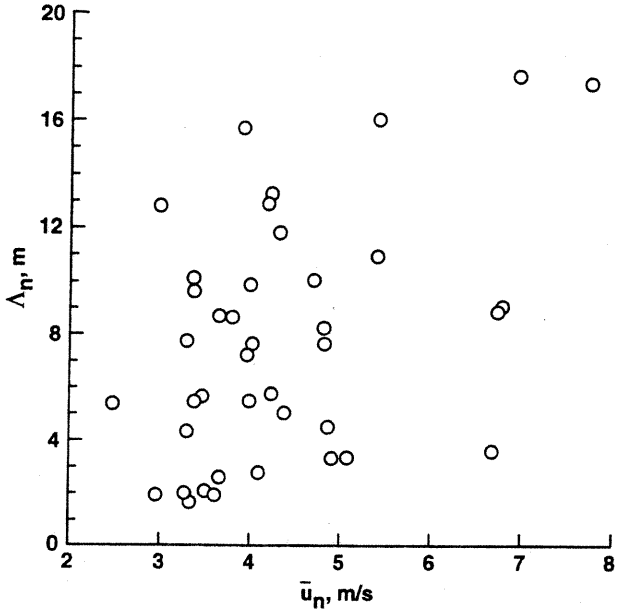

Fig. 11. Near-field longitudinal eddy length.

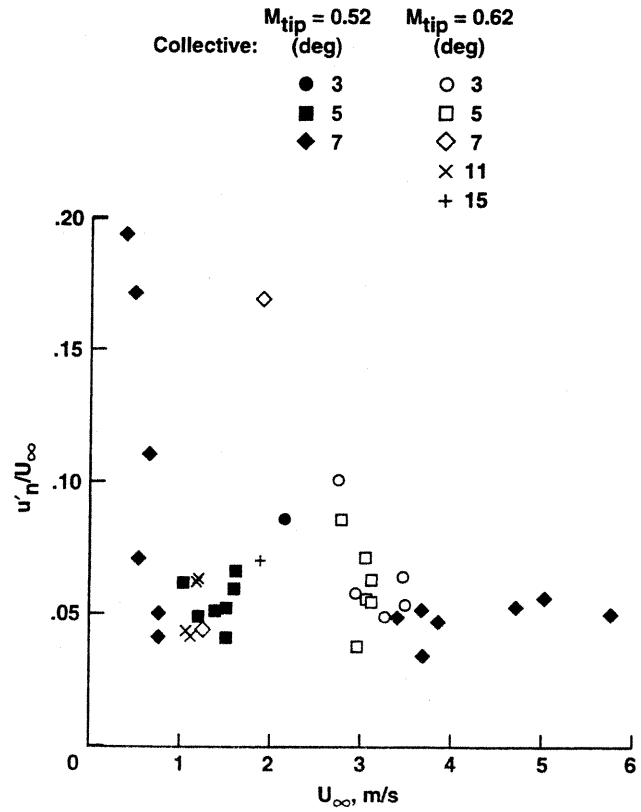

Fig. 12. Near-field rms turbulence velocity.

Acoustic Measurements

Acoustics results are discussed for two observer positions, mic 6 and mic 9 (Table 1 and Fig. 3). The primary measurement location, microphone 9, was on the rotor axis 4.5 rotor radii from the rotor. Measurements at this location show the greatest effect of atmospheric turbulence ingestion. Microphone 6 was located 90° (in-plane) from the rotor axis. Background noise measurements were typically at least 20 dB below the acoustic measurements of the rotor, therefore no corrections were made for background noise.

General characteristics of the measured noise are discussed first. Next, atmospheric effects on measured noise are presented. Variations in ingested rms turbulence velocity, atmospheric wind speed, and inflow velocity are investigated to determine their influence on the rotor noise. No distinct effect of eddy length on measured noise was observed. Effects of varying rotor thrust are then discussed, followed by a discussion of the effects of inserting a turbulence-generating grid upstream of the rotor.

General Characteristics. Fig. 4 shows an averaged spectrum from microphone 9 with and without the gear noise removed. The mean ambient wind for this condition is essentially zero; however, zero mean ambient wind does not preclude the existence of turbulence. The near-field tower was not installed for this condition. Several aspects of this spectrum are characteristic of the noise measured in this experiment. The spectrum contains numerous distinct rotor blade passage harmonics rising above the broadband noise. For a hovering rotor, two mechanisms which produce peaks at the blade passage frequency harmonics are steady loading noise and turbulence ingestion noise. Peaks from steady loading noise diminish with increasing frequency much faster than in this example. The peaks in the measured spectrum are very narrow at the lower frequencies and increase in width as the frequency increases; this is a characteristic of turbulence ingestion noise (Ref. 17). Another possible cause of widening peaks is unsteadiness in the rotor speed; however, as explained earlier, the rotor speed was found to be very steady. Also, the peaks identified with the gear noise do not widen at the higher frequencies. Therefore, the widening of the peaks in the spectrum is most likely caused by turbulence ingestion. Additional spectra from microphone 9 acquired for various rotor and atmospheric conditions exhibit similar characteristics. In contrast, spectra from microphone 6 (in-plane location) exhibit different characteristics, as shown in Fig. 13. The amplitudes of the first 2 or 3 blade passage harmonics are larger and can be attributed to thickness noise. Amplitudes diminish quickly for the first 3 or 4 harmonics; generally, levels of all harmonics above about the fourth are lower at this location. The existence of distinct and broadening peaks in the spectra out to 2 kHz suggest some noise could be radiating from the turbulence ingestion; however, this noise is about 40 dB below the fundamental and thus contributes little to the sound level in the plane of the rotor either in OASPL or dBA measurements.

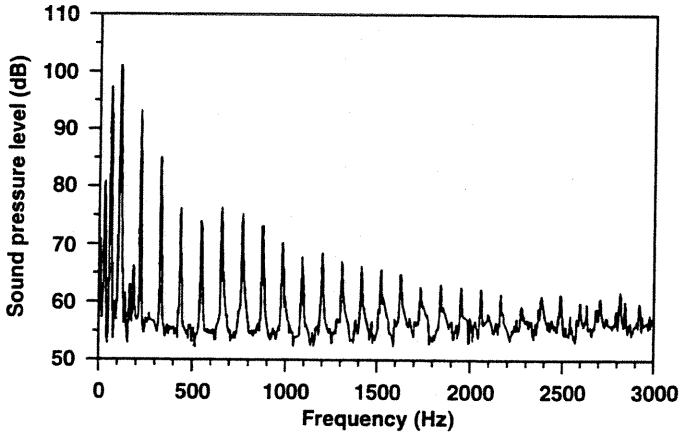

Fig. 13. Power spectrum for Run 44 Point 5, M_{tip} = 0.56, θ = 11°, U_∞ = 0.00 m/s, near-field tower not installed, grid not installed, Microphone 6.

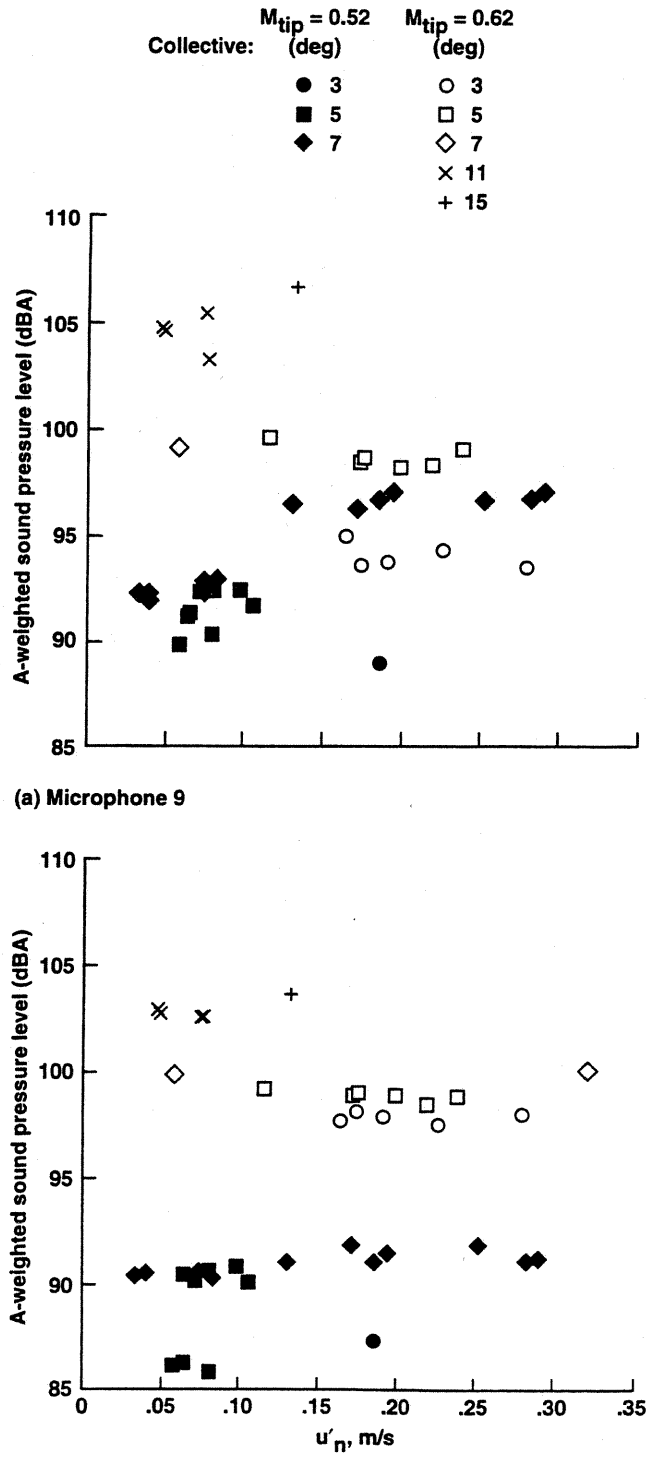

Fig. 14. Measured sound level variation with rms turbulence velocity, near-field tower installed, grid not installed. (a) Microphone 9, (b) Microphone 6.

Atmospheric Turbulence Effects. Variations in atmospheric turbulence are expected to cause changes in sound measurements when turbulence ingestion is a major sound-producing mechanism. The structure of the inflow turbulence incident on the rotor will influence the nature of the blade lift fluctuations and thus the radiated sound. If the time records of the probes were long enough to obtain a statistical average and short enough for the turbulence characteristics to be quasi-stationary, the near- and far-field measured turbulence characteristics should be clearly related. As shown in Fig. 8, however, much scatter exists in the atmospheric (far-field tower) turbulence measurements. In this section, therefore, acoustic measurements will be related to estimates of turbulence characteristics made in the near-field.

When a rotor interacts with atmospheric turbulence, the turbulence produces fluctuating pressures on the rotor blades leading to fluctuating lift and drag. These pressure fluctuations radiate away from the rotor as sound. Most likely, the fluctuating lift will be greater than the fluctuating drag. If this happens, the radiated sound will be most dominant perpendicular to the blade surface in the direction of the rotor axis rather than parallel to the blade surface, in the plane of the rotor. Also, higher rms turbulence velocities are expected to produce higher pressure fluctuations and higher radiated sound levels than lower rms turbulence velocities would produce. Fig. 14 shows the effects of rms turbulence velocity in the near-field, u'_n, on the sound radiated by the rotor for two values of M_{tip}. The turbulence-generating grid was not present. The metric dBA was chosen over OASPL because dBA gives more weight to frequencies between 1 and 4 kHz. Turbulence ingestion noise in this frequency range, where humans are most sensitive, is more significant than thickness or steady loading noise. There appears to be little or no trend with rms turbulence velocity for either of the microphones at either M_{tip}. At the in-plane location (mic 6), thickness noise dominates the radiated noise and is manifested mainly in the first few rotor harmonics. Although Fig. 14 does not reveal a significant correlation of sound level with u'_n, power spectra can reveal more detailed information.

Fig. 15 shows spectra from two points in Fig. 14 with a collective pitch of 7°, M_{tip}=0.52, and two different values of u'_n. All other conditions for the two points are similar, except the atmospheric wind speed. The wind speeds are 0.7 and 3.9 m/s corresponding to the smaller and larger values of u'_n, respectively. The on-axis microphone (Fig. 15(a)) shows that with higher u'_n, the amplitude of the lower frequency rotor blade passage harmonics is greater than for the lower u'_n case; the amplitudes of the higher frequency harmonics are about the same. Also, with higher rms turbulence velocities, the broadband noise floor increases, about 2 dB at the lower frequencies and about 5 dB at the higher frequencies shown. The in-plane microphone (Fig. 15(b)) does not appear to be significantly influenced by the change in u'_n.

As stated earlier, no distinct effect of eddy length on rotor noise was found. An explanation of this follows. The rotor is expected to chop the eddy 80 to 800 times, because of the high rotational velocity of this tail rotor (blade passage frequencies of 102-124 Hz) and the ingested eddy size (2 to 20 m). Chopping an eddy 80 times is sufficient to produce fairly coherent sound; increasing the number of interactions above 80 may have insignificant effect on the coherence. Thus noise produced by the tail rotor chopping of the longest eddies may be only slightly more coherent than the noise produced by the rotor chopping the shortest eddies in this experiment.

The atmospheric wind speed is the other basic characteristic of the atmospheric turbulence that was measured. The normalized rms turbulence velocities in the near-field and far-field are independent of atmospheric wind speed (Figs. 9 and 12). Fig. 16 shows acoustic measurements for M_{tip}=0.52 and 0.62 without the grid present. Results are similar to those observed in Fig. 14. Again, levels increase with increasing rotor collective pitch.

Rotor Inflow. Measured sound levels correlate more strongly with the rotor inflow velocity than with any other parameter or atmospheric quantity measured.

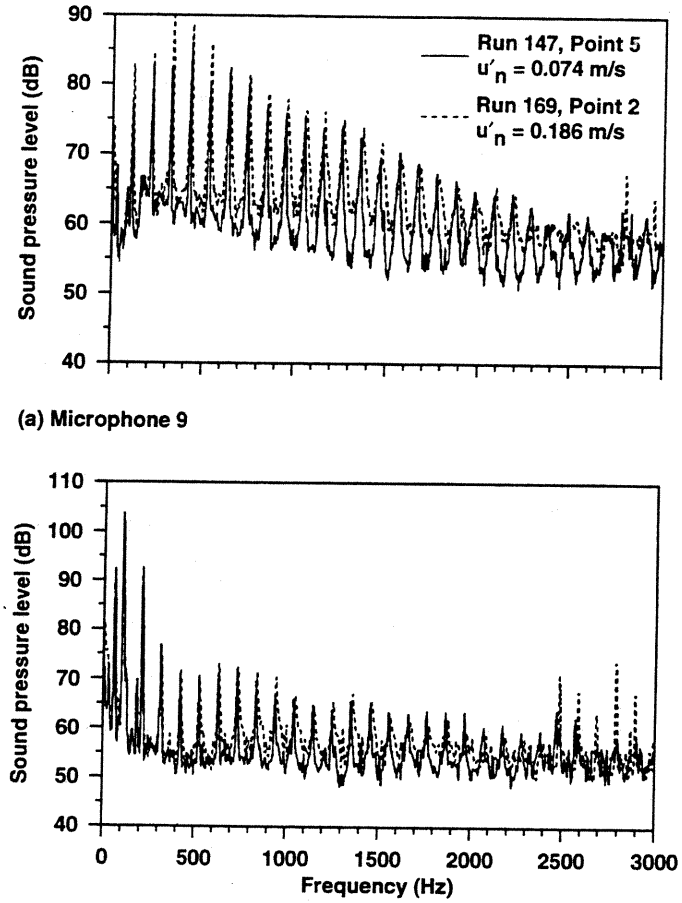

Fig. 15. Effect of near-field rms turbulence velocity on acoustic power spectra for $\theta = 7°$, Mtip = 0.52, near-field tower installed, grid not installed. (a) Microphone 9, (b) Microphone 6.

At the microphone location on the rotor axis (Fig. 17(a)), sound levels measured in dBA increase with increasing rotor inflow velocity without the grid present. The strong dependence on rotor inflow velocity suggests that an obstruction to the inflow might be causing noise by producing disturbances that the rotor chops. This possibility was eliminated by examining sound data acquired with the rotor thrusting in the opposite direction (negative C_T/σ).

In the rotor plane (Fig. 17(b)), a slight trend of increasing sound levels with increasing inflow velocity occurs. Also, in the rotor plane where thickness noise radiates strongly, the tip Mach number influences the sound level more than at the other microphone locations. The previous discussion (see the "Data Quality" section), indicated that no obstruction contributed significantly to the sound levels for the in-plane microphone.

Rotor Thrust. Increasing rotor thrust will obviously increase the loading noise of the rotor; however, according to current theories (Refs. 15 and 18), pressure disturbances on the rotor blade (and hence radiated sound) due to turbulence ingestion are independent of the steady lift of the rotor blade. Since the current theories are based on linearized flow on airfoils, there is no direct influence of thrust on the propagation of noise caused by turbulence ingestion. Our observations suggest a more complete theory is needed to predict the propagation of noise caused by turbulence ingested into a rotor. In these current theories,

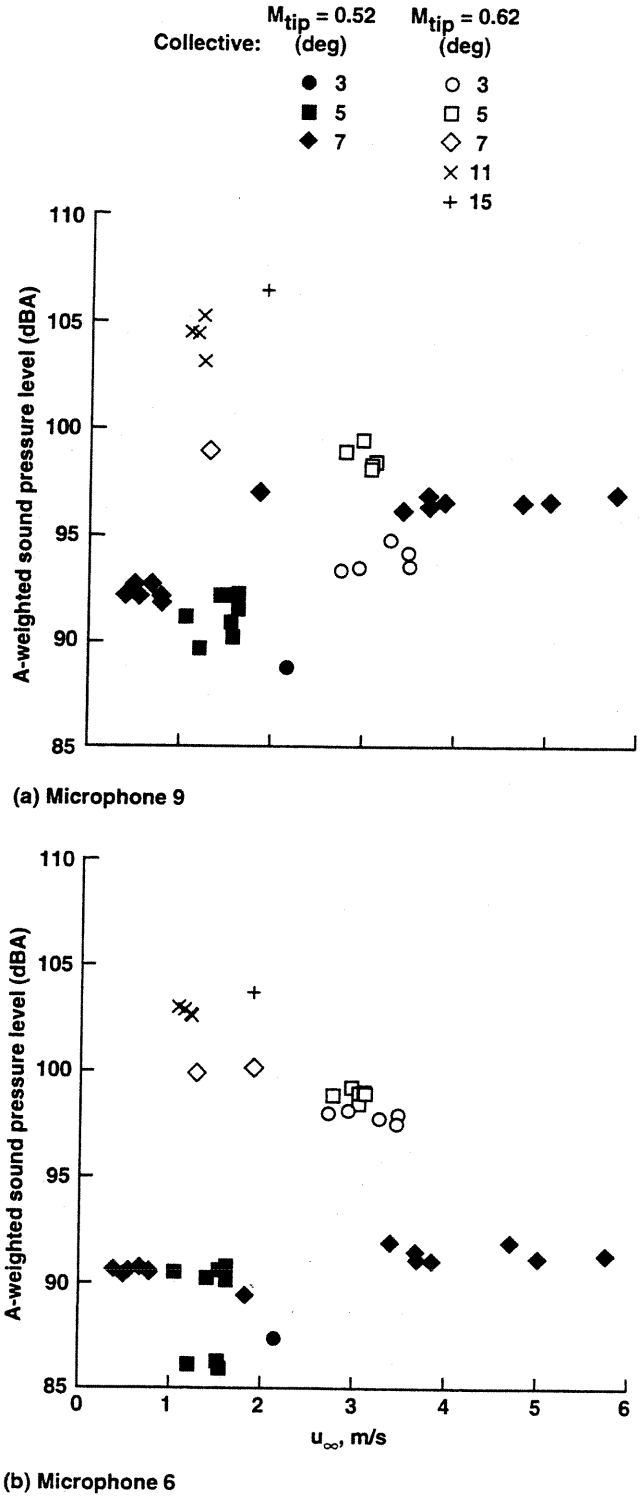

Fig. 16. Measured sound level variation with atmospheric wind speed. Near-field tower installed, grid not installed. (a) Microphone 9, (b) Microphone 6.

increasing rotor thrust increases the eddy length distortion, producing longer longitudinal eddies. With the same energy in the eddy distributed over a longer eddy, the expected effect on noise is to produce more blade-to-blade correlation. The total acoustic energy remains the same and is more concentrated at the blade passage harmonics because of the

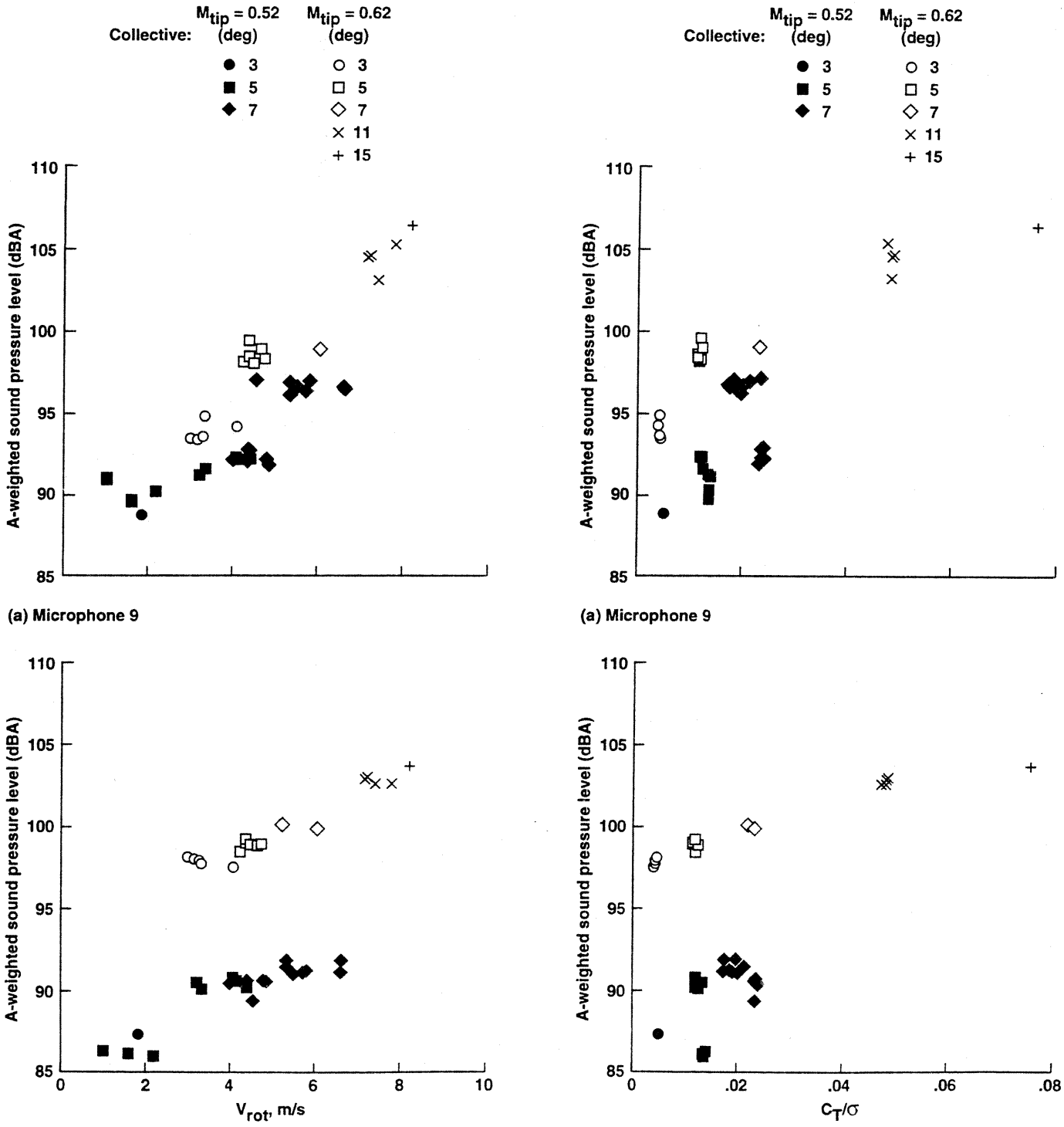

Fig. 17. Measured sound level variation with rotor inflow velocity. Near-field tower installed, grid not installed. (a) Microphone 9, (b) Microphone 6.

Fig. 18. Measured sound level variation with C_T/σ, near-field tower installed, grid not installed. (a) Microphone 9, (b) Microphone 6.

increase in blade intersections with a given eddy. In all the measurements examined above, however, the sound level in dBA increased with increasing rotor collective. As explained earlier, the metric dBA was chosen to emphasize the frequency range of turbulence ingestion noise rather than steady loading noise. The collective pitch directly influences the rotor C_T/σ, a more direct measure of how the rotor interacts with the air. Fig. 18 shows sound pressure level measured in dBA as a function of C_T/σ. The grid was not present. Along the rotor axis (mic 9, Fig. 18(a)), the sound level increases with increasing C_T/σ. In the plane of the rotor (mic 6, Fig. 18(b)) the sound levels increase with increasing C_T/σ, but not as steeply as compared to mic 9.

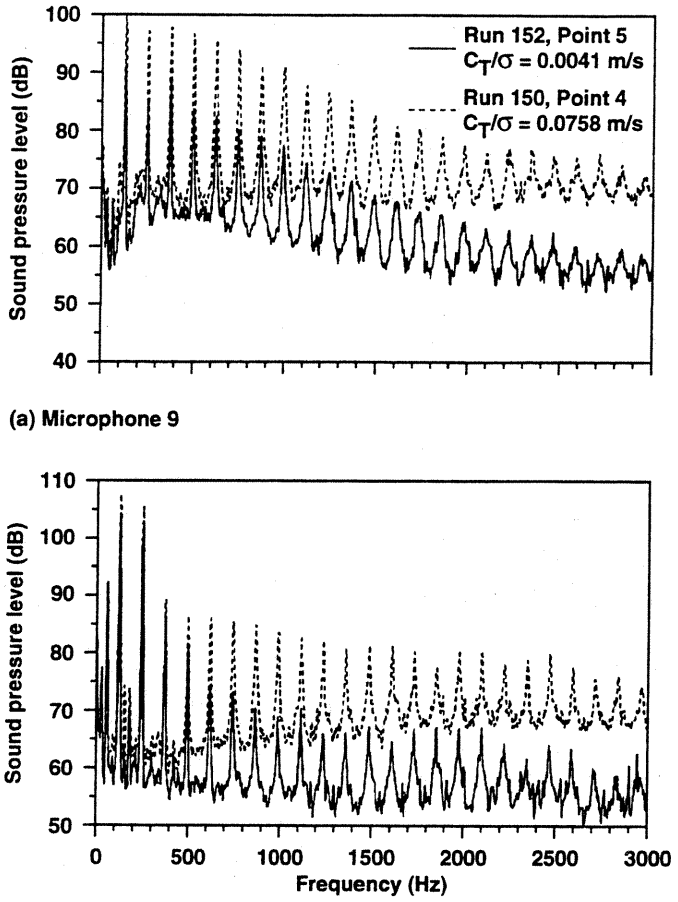

Fig. 19. Effect of C_T/σ on acoustic power spectra. Near-field tower installed, grid not installed. (a) Microphone 9, (b) Microphone 6.

Fig. 19 shows spectra from two points in Fig. 18 for M_{tip}=0.62. Spectra are shown for collectives of 3° and 15° corresponding to C_T/σ of 0.004 and 0.076, respectively. Amplitudes of the low-order blade passage harmonics increase 5 to 10 dB from low to high thrust, for mic 9 (Fig. 19(a)). The increase is less at the in-plane location (Fig. 19(b)). Loading noise dominates the low-order harmonics at the on-axis location and thickness noise dominates at the in-plane location. Amplitudes of higher frequency harmonics increase 10 to 15 dB at both locations with increased thrust. Measurements in dBA (Fig. 18) also increase 10 to 15 dB. The broadband floor is a few dB higher at the higher frequencies. These observations indicate turbulence ingestion as the mechanism associated with the higher harmonics.

Turbulence Grid. A grid in a fluid stream creates eddies with length scales on the order of the grid spacing. These eddies decay far downstream of the grid. In this test, the rotor was in the near downstream region of the grid where the small, grid-generated eddies had partially decayed but the larger atmospheric eddies had not yet been significantly affected by the introduction of the grid-generated small-scale turbulence. Inserting the grid changed the turbulence ingested by the rotor. Although the exact nature of this change was not documented, the grid added small-scale turbulence to the existing atmospheric turbulence. This change in turbulence is expected to increase the broadband floor of the noise spectra in the higher end of the spectrum examined in this investigation. Fig. 20 shows measurements for M_{tip}=0.62 with and without the grid present for θ=3°, 7°, and 15°. Except in the plane of the rotor, noise measurements with the grid present are consistently higher. Measured values of u'_n are not available for conditions with the grid, but Batchelor (Ref. 9) provides an equation for estimat-

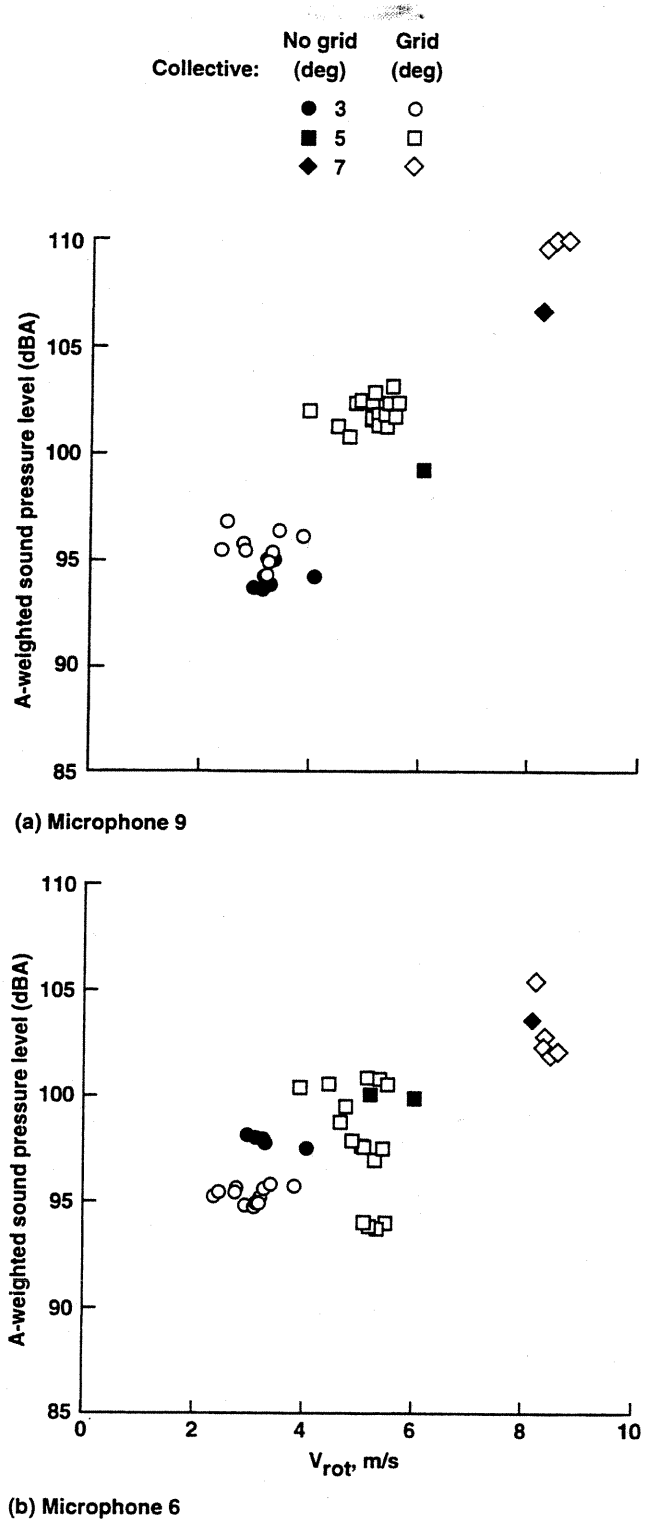

Fig. 20. Effect of grid on meaured sound level variation. Near-field tower installed. (a) Microphone 9, (b) Microphone 6.

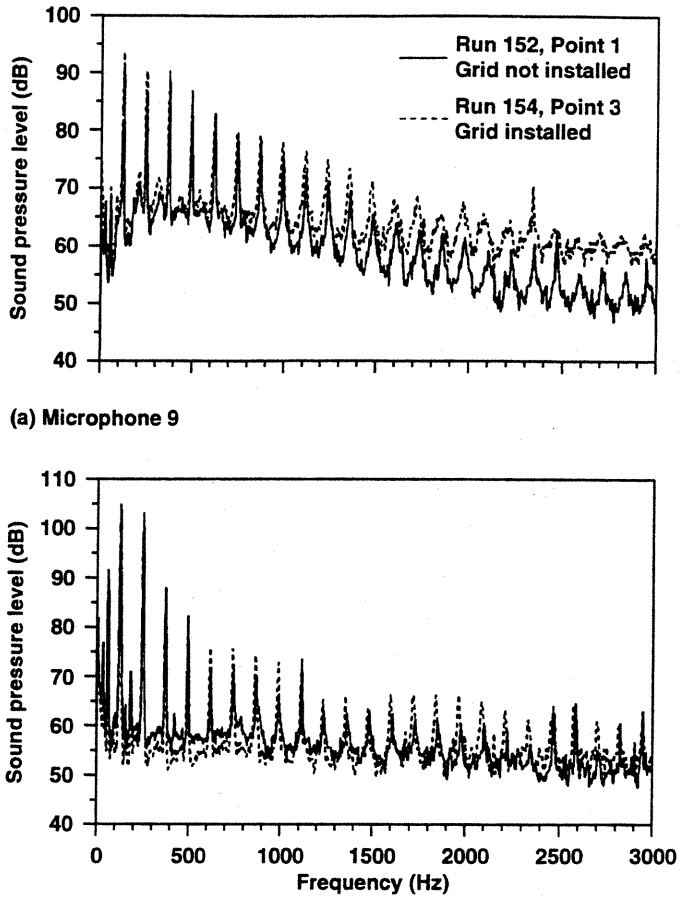

Fig. 21. Effect of grid on acoustic power spectra for $\theta = 3°$. Near-field tower installed, (a) Microphoen 9, (b) Microphone 6.

ing the rms turbulence velocity downstream of a grid:

$$\left(\frac{\bar{u}}{u'}\right)^2 = 134\left(\frac{g}{d} - \frac{g_0}{d}\right)$$

The calculated rms turbulence velocities range from 0.067 to 0.26, 0.12 to 0.36, and 0.19 to 0.53 for θ=3°, 7°, and 15°, respectively. The error in estimating g_0/d has been included in these calculations, i.e., $5 \le g_0/d \le 15$. Fig. 21 shows spectra, with and without the grid, representing two points in Fig. 20 for a collective pitch of 3°. For mic 9 (Fig. (21(a)), amplitudes of the rotor blade passage harmonics are 3 to 5 dB higher for most harmonics when the grid is present. The amplitude of the broadband floor is also higher with the grid, about 3 dB at low frequencies and increasing with increasing frequency.

Conclusions

This investigation examined some of the effects of atmospheric turbulence ingestion on hovering tail rotor acoustics. The presentation of dBA levels and power spectra provide overall and detailed information concerning changes in radiated sound due to various atmospheric parameters. The data clearly indicate a strong dependence of measured sound levels on the rotor inflow velocity and thrust level. This trend is somewhat unexpected and warrants further investigation. The following conclusions, based on two fixed-location hot-film probes and two fixed-location microphones, are drawn from the presented data.

1) Sound levels measured in dBA increase with increasing rotor inflow velocity and rotor thrust. Current linear theories do not account for the influence of rotor thrust on turbulence ingestion noise.

2) Normalized far-field rms turbulence velocity is independent of atmospheric wind speed.

3) Normalized near-field rms turbulence velocity is independent of atmospheric wind speed. There is no discernible effect of rotor operating condition on the rms turbulence velocity.

4) The widening of peaks with increasing frequency in the measured spectrum is attributed to turbulence ingestion noise.

5) Noise measurements made along the rotor axis indicate that with higher near-field rms turbulence velocity, the amplitude of the lower frequency rotor blade passage harmonics is greater than for the lower u'n case; the amplitudes of the higher frequency harmonics are about the same. Also, with higher near-field rms turbulence velocity, the broadband noise floor increases, about 2 dB at the lower frequencies and about 5 dB at the higher frequencies.

6) No distinct effect of eddy length on measured noise was observed.

7) No distinct effect of atmospheric wind speed on measured noise was observed.

8) The addition of small scale turbulence caused by installing a grid upstream of the rotor increased the sound levels, measured in dBA, for the location on the rotor axis. Also, the amplitude of the broadband floor in the measured spectrum is higher with the grid.

Acknowledgments

The authors thank Dr. Charles Smith of NASA Ames for his helpful comments and suggestions. We also appreciate the informative discussions with Dr. Dennis Thomson of Pennsylvania State University, Dr. Doug Westphal of NASA Ames Research Center, and Mr. Mike Marcolini of NASA Langley Research Center.

References

[1]George, A. R., "Helicopter Noise: State-of-the-Art," *Journal of Aircraft,* Vol. 15, (11), pp. 707-715, Nov 1978.

[2]Janakiram, R. D., "Aerodynamics of Rotorcraft," AGARD Report No. 781, Nov 1990.

[3]Hagen, M. J., Yamauchi, G. K., Signor, D. B., and Mosher, M., "Measurements of Atmospheric Turbulence Effects on Tail Rotor Acoustics," NASA TM 108843, Sept 1994.

[4]Signor, D., Yamauchi, G., Smith, C., and Hagen, M., "Performance and Loads Data from an Outdoor Hover Test of a Lynx Tail Rotor," NASA TM 101057, June 1989.

[5]Gregory, N., and Wilby, P. G., "NPL 9615 and NACA 0012, A Comparison of Aerodynamic Data," NASA CP 1261, 1973.

[6]Owen, T. B., and Beauchamp, A. R., "Aero-Acoustic Measurements on a Lynx Tail Rotor in the RAE 24ft Wind Tunnel," RAE-TM-Aero-1972 (X84-70842), July 1983.

[7]Signor, D. B., Yamauchi, G. K., Mosher, M., Hagen, M. J., and George, A. R., "Effects of Ingested Atmospheric Turbulence on Measured Tail Rotor Acoustics," AHS 48th Annual Forum, Washington D. C., June 1992.

[8]Hinze, J. O., *Turbulence,* McGraw Hill, Inc., 1975, pp. 259-277.

[9]Batchelor, G. K., *The Theory of Homogeneous Turbulence,* Cambridge University Press, 1967, pp. 133-168.

[10]Dale, A. K., "Gear Noise and The Sideband Phenomenon," ASME Design Engineering Tech. Conf., Cambridge, MA, Oct 7-10, 1984.

[11]Paterson, R. W., and Amiet, R. K., "Noise of a Model Helicopter Rotor Due to Ingestion of Turbulence," NASA CR 3213, Nov 1979.

[12]Simonich, J. C., Schlinker, R. H., and Amiet, R. K., "Experimental Assessment of Helicopter Rotor Turbulence Ingestion Noise in Hover," NASA CR 181792, June 1989.

[13]Thomson, D. W., and Henderson, H. W., "Definition of Local Atmospheric Attractors using Measurements Made with Surface-based Remote Sensing Systems," First Experimental Chaos Conference, Arlington, Virginia, Oct 1-3, 1991.

[14]Wilson, D. K., "Propagation of Sound Through the Fluctuating Atmosphere," Second International Congress on Recent Developments in Air- & Structure-Borne Sound and Vibration, Auburn, Alabama, Mar 4-6, 1992.

[15]Simonich, J. C., Amiet, R. K., Schlinker, R. H., and Greitzer, E. M., "Helicopter Rotor Noise Due to Ingestion of Atmospheric Turbulence," NASA CR 3973, May 1986.

[16]Panofsky, H. A., and Dutton, J. A., *Atmospheric Turbulence,* John Wiley & Sons, 1984, pp. 87, 139-140.

[17]Homicz, G. F., and George, A. R., "Broadband and Discrete Frequency Radiation for Subsonic Rotors," *Journal of Sound and Vibration,* Vol. 36, (2), pp. 151-177, 1974.

[18]Amiet, R.K., "Noise Produced by Turbulent Flow Into a Rotor: Theory Manual for Noise Calculation," NASA CR 181788, June 1989.